4.3 Retention of radionuclides by secondary phase formation

F. Heberling, N. Finck, Z. Nie, C. Garcia, T. Hippel, P. Lindqvist-Reis, K. Dardenne

In co-operation with:

N. Bogachev[a]

[a] Saint Petersburg State University, Saint Petersburg, Russia

Introduction

During the (geo)chemical evolution of a nuclear waste repository, ground water may migrate through the geological and geotechnical barriers and reach the technical barrier encapsulating the nuclear waste. In aqueous environments, various secondary phases may form as alteration or corrosion products of materials from the multi-barrier system or the waste matrix itself. Steel canisters and the waste glass are expected to corrode/alter over extended periods of time in contact with ground water and various Fe-bearing secondary phases will form, such as for example iron (hydr)oxides and iron containing clay minerals. Calcite on the other hand is expected to form as an alteration product of concrete based materials and also may be present as a constituent of possible host rock formations (e.g. argillites).

Secondary phases have the potential to scavenge radionuclides (RNs) and to retard their migration to the biosphere. Various molecular scale retention processes, from surface adsorption to structural incorporation have been reported. Especially structural incorporation, i.e. solid-solution formation, is argued to lead to a significant retention of the RNs in the near field of a repository. However, despite the abundance of solid-solutions found in natural systems, reliable thermodynamic and kinetic models to predict their formation are hardly available.

The group working on secondary phases at INE aims at developing quantitative thermodynamic models based on a molecular scale process understanding, by combining information from specific laboratory experiments with information from advanced spectroscopic, microscopic, and diffraction techniques as well as computational studies. Thus, we investigate the structural incorporation of RNs into various secondary phases expected to form in the multi-barrier system around potential nuclear waste repositories. Detailed below are two examples: Ln/An(III) uptake by calcite and a study characterizing structural iron in clay minerals.

Eu^{3+} incorporation into calcite

Eu^{3+}, Cm^{3+}, and Am^{3+} uptake by calcite is a subject of investigations by the KIT-INE secondary phases group since several years. Besides the relevance of this system for the potential retention of long-lived trivalent actinide elements in the multi-barrier system, especially Eu^{3+} and Cm^{3+} in calcite provide ideal substrates for investigations with time resolved luminescence spectroscopy. Especially since we have the possibility to perform site-selective, direct excitation measurements at low temperature (< 20 K) (e.g. [1]) detailed information on the incorporation species has been obtained. First studies relied on calcite syntheses in Mixed Flow Reactors (MFR) at steady state conditions. Marques et al. (2008) [2] investigated the influence of the available surface area in the MFR and the background electrolyte cations (Na^+, K^+), which are available to provide charge compensation in the potential incorporation mechanism where two Ca^{2+} ions in calcite are replaced by one Eu^{3+} and one Na^+/K^+. In contrast to Na^+, the larger K^+ ion is incompatible with the calcite structure and distorts the local structure upon charge compensation. Marques et al. report three incorporation species A, B, and C.

Species C is identified as a well-ordered incorporation species. The corresponding $^7F_0 \rightarrow {}^5D_0$ transition is excited at 579.5 nm. The twofold crystal field splitting of the $^5D_0 \rightarrow {}^7F_1$ transition and the threefold splitting of the $^5D_0 \rightarrow {}^7F_2$ transition, detected for the sample synthesized in the presence of Na^+, are in line with Eu^{3+} occupying a Ca^{2+} site in the calcite structure (D_{3d} symmetry). For the sample synthesized in the presence of K^+, Marques et al. report threefold splitting of the $^5D_0 \rightarrow {}^7F_1$ band and a fivefold splitting of the $^5D_0 \rightarrow {}^7F_2$ band, due to a lowering of the symmetry of the local structural environment of Eu^{3+} in calcite due to charge compensation by the large K^+ cation. Species C has a long fluorescence lifetime (> 3 ms), indicating no coordinating water [3].

Species B is another incorporation species, as identified by the long fluorescence lifetime (> 3 ms, [3]). Species B is characterized by a low-symmetry coordination environment, compared to species C as indicated by the full crystal field splitting of the $^5D_0 \rightarrow {}^7F_1$ and $^5D_0 \rightarrow {}^7F_2$ bands. Species B is excited at 578.4 nm. It has a very characteristic $^5D_0 \rightarrow {}^7F_2$ transition spectrum with a sharp emission peak around 619 nm. A fact not mentioned by Marques et al, but obvious from their spectra is, that the formation of species B seems to be enhanced in the presence of K^+ compared to the synthesis in the presence of Na^+.

Species A is excited at 578.1 nm, it has a substantially lower fluorescence lifetime (0.46 ms) compared to species B and C. This lifetime would be in line with one or two water molecules coordinated to the Eu^{3+} ion [3]. The ratio between species B and C on the one hand side and species A on the other hand side increased strongly upon a decrease of the reactive

surface area in the MFR. Thus, species A is interpreted as a surface species.
In a follow up study calcite was synthesized by recrystallization of metastable vaterite to the more stable polymorph calcite [4]. Here an additional transition species, which we will denote as species D here, was introduced. Species D was detected at early stages of calcite formation. It has a fluorescence lifetime of 1.1 ms, corresponding to 0.3 coordinating water molecules.

In a later study, Hofmann et al. reported on the effect of NO_3^- on Eu^{3+} incorporation into calcite [10]. Besides Eu doped calcite synthesized in MFR experiments Hofmann et al. report results of batch sorption experiments. Compared to the previous studies, Eu containing calcite synthesized in the presence of $NaNO_3$ in the MFR or in batch sorption experiments (in the presence of $NaNO_3$ or $NaClO_4$) show no well-defined species with sharp absorption peaks. Instead, excitation spectra are characterized by broad peaks, which shift slightly depending on the background electrolyte anion or the addition order of NO_3^- and Eu^{3+}.

In a most recent study Hellebrandt et al. report on calcite recrystallization in the presence of Eu^{3+} [5]. For short reaction times and low reactive surface areas they find broad peaks in excitation spectra similar to Hofmann et al.. For longer reaction times and small calcite particles with large reactive surface areas sharper bands are reported. Among these, species B is reproduced quite clearly and an additional species with similarities to species D is reported.

Here we report on Eu^{3+} incorporation into calcite upon recrystallization of calcite and aragonite. Aragonite is a less stable polymorph of $CaCO_3$ at standard conditions compared to calcite. Thus, aragonite dissolves in aqueous solution to transforms to the more stable calcite. In the pure calcite system, rough irregular calcite particles transform via dissolution-reprecipitation processes to more stable idiomorphic calcite crystals [6].

Experimental details

We performed calcite recrystallization experiments in a kinetic series in 0.01 M NaCl solution at 5 µM initial Eu^{3+} concentration, and in a second and third experimental series in various background electrolytes ($NaBrO_3$, $NaClO_4$, NaI, NaBr, NaCl, $NaNO_3$, and KCl) at 0.1 M concentration and 1 µM initial Eu^{3+} concentration. The aragonite-calcite recrystallization study was a long-term experiment in 0.1 M NaCl solution at 0.76 µM initial Eu^{3+} concentration. For the calcite recrystallization experiments in the presence of various background electrolyte anions and the kinetic series, we follow the course of recrystallization by ^{45}Ca exchange measurements as previously described [6]. The solid / liquid ratio is 2 g/L in the calcite recrystallization experiments, and 20 g/L in the aragonite experiment.

Spectroscopy is performed using a Dye Laser (Radiant Dyes Laser) pumped by the second harmonic (532 nm) a Nd:YAG Laser (Continuum). The used dye, Pyrromethene 597, allows to adjust the excitation wavelength in a range from 582 nm to 575 nm, the range relevant for direct excitation of the Eu^{3+} $^7F_0 \rightarrow {}^5D_0$ transition. The sample is cooled to 4 - 6 K in a He-cryostat (CryoVac) at ~10^{-8} mbar. Luminescence is recorded on an intensified CCD camera coupled to an Andor spectrometer employing a 1200 lines/mm grating. The full setup is controlled by a homemade Labview software.

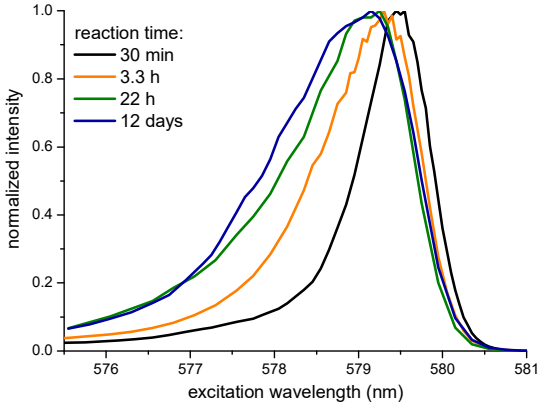

Fig. 1: *TRLFS excitation spectra of Eu^{3+} in Calcite recrystallized in the presence of 0.01 M NaCl. Spectra are recorded after various reaction times.*

Results

Spectra measured on samples from the kinetic experiment are shown in Figure 1. The excitation spectra show a continuous trend towards excitation at lower wavelength with increasing reaction time. Luminescence spectra recorded at various excitation wavelength (not shown here) demonstrate that except for the first sampling time (30 min) the Eu species in the various samples are very similar. According to ICP-MS Eu^{3+} concentration, and LSC ^{45}Ca concentration measurements (results not shown), the Eu^{3+} uptake in the system is very fast, while ^{45}Ca uptake is sequentially increasing over the 14 days' reaction period. For the sample taken after 30 min this means that Eu^{3+} is obviously already bound to the surface, while calcite transformation has not yet started. This nicely explains the clearly different spectroscopic signature of the sample taken after 30 min. At later stages ^{45}Ca data indicate a sequential increase from 1.5% and 7.5% calcite recrystallization, which would correspond to 5 to 28 monolayers. This continuous recrystallization, which is not accompanied with a measurable decrease in Eu^{3+} solution concentration, does not lead to substantial changes in the emission spectra.

Results of the second experimental series are shown in Fig. 2. In this experimental series, the influence of the background electrolyte anion is investigated. The initial Eu^{3+} concentration is lower than in the previous series (1 µM instead of 5 µM). Spectra are recorded after 14 days of reaction time. At that time 16% of calcite recrystallized. The overall reaction progress does not vary significantly with the background electrolyte.

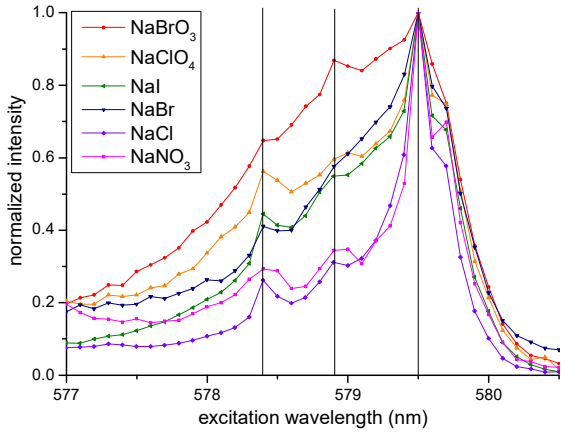

Fig. 2: *TRLFS excitation spectra of Eu^{3+} in calcite, recrystallized in various background electrolytes. Vertical lines highlight the peak positions assigned to species B (578.4 nm), D (578.9 nm), and C (579.5 nm).*

As shown in Fig. 2, we observe the formation of more well defined species with sharp peaks at 578.4 nm, 578.9 nm, and 579.5 nm compared to the spectra in Fig 1. It is interesting to note that despite very similar overall recrystallization rates, the degree to which distinct well-defined Eu^{3+} incorporation species form, seems to vary with the background electrolyte anion. Thus, as previously described [7], the background electrolyte anions must in a way affect interfacial kinetics. Still we consider it more important to point out the similarities between the samples. Emission spectra (not shown) after excitation at 578.4 nm clearly show a sharp peak close to 619 nm, characteristic for the previously described species B [2]. After excitation at 578.9 nm luminescence shows similarities to spectra in the previous experimental series, and to species D [4]. The $^5D_0 \rightarrow {}^7F_2$ emission after excitation at 579.5 nm nicely exhibits threefold splitting, characteristic for the previously described species C [2].

In a third experimental series, we investigated the influence of the background electrolyte *cation*. Fig. 3 shows the corresponding $^5D_0 \rightarrow {}^7F_1$ and $^5D_0 \rightarrow {}^7F_2$ emission spectra recorded after excitation at 578.4 nm (species B) and 579.5 nm (species C) for two samples prepared in the presence of NaCl and KCl, respectively. Thus, we reproduce the effects discussed above with respect to the work by Marques et al.: the formation of species B (characteristic sharp F_2 emission peak around 619 nm) is more pronounced in the KCl system, while the centro-symmetric species C (twofold split F_1 band, and threefold split F_2 band) forms only in the presence of Na^+, and becomes distorted if only K^+ is available for charge compensation.

Results of the long-term aragonite to calcite recrystallization experiment are shown in Fig. 4. After 400 days' recrystallization, all aragonite had transformed to calcite according to powder XRD. No additional mineral phase was detected. The initially measured excitation spectrum exhibits only one sharp peak at 579.50 nm, which perfectly corresponds to species C, also regarding the emission spectrum. A more detailed measurement, however, revealed that there are two peaks, one at 579.50 nm, and one extremely sharp and intense peak at 579.58 nm, in the following denoted as species C'. According to the fluorescence lifetime (1.8 ms, < 0 coordinating water molecules [3]), species C' seems to be an incorporated Eu-species.

Demixing and formation of a separate Eu-phase cannot be ruled out completely. However, on the basis of XRD results and the fact that a pure Eu-phase would be expected to exhibit an even shorter fluorescence lifetime due to concentration quenching, this explanation seems unlikely. The observed crystal

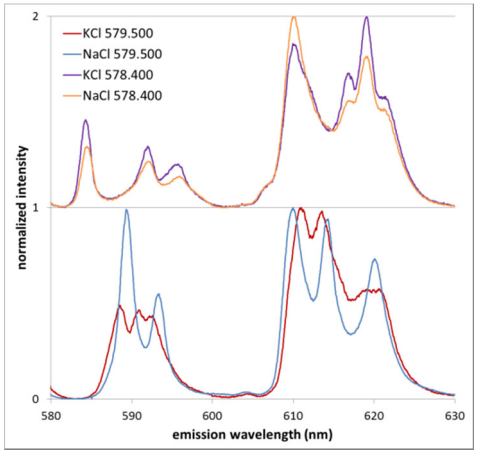

Fig. 3: *TRLFS emission spectra of Eu^{3+} in calcite, recrystallized in presence of NaCl and KCl, respectively. Luminescence is recorded after excitation at 578.40 nm and 579.50 nm as indicated in the Figure legend. $^5D_0$-$^7F_1$ emission corresponds to peaks between 585 nm and 600 nm, $^5D_0$-$^7F_2$ emission corresponds to peaks between 606 nm and 630 nm. Note the small peak around 604 nm, a vibronic sideband caused by coordinating carbonate ligands.*

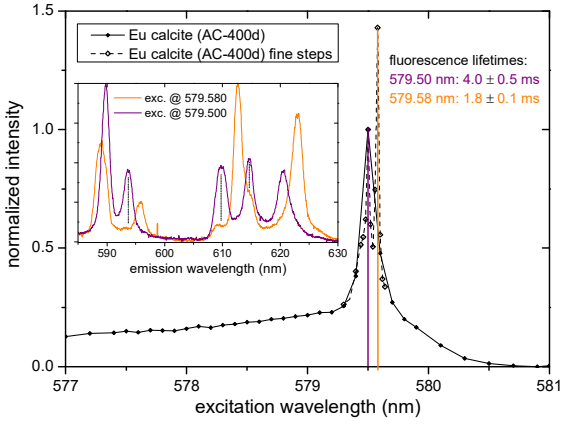

Fig. 4: *Spectra recorded on the Eu-doped calcite sample obtained from the long-term aragonite to calcite recrystallization experiment after 400 days, denoted AC-400d. The main graph shows excitation spectra measured with different step sizes. Note that the intensity of the detailed spectrum was adjusted to match the main peak of the spectrum measured with coarse steps. The insert shows corresponding emission spectra after excitation at the two peak maxima at 579.50 nm and 579.58 nm.*

Tab. 1: *Eu-species identified in calcite*

	Species B	Species D	Species C	Species C'
excitation wavelength	578.40 nm	~ 579 nm	579.50 nm	579.58 nm
lifetimes (ms)	(0.9 ± 0.1) 4 ± 1	0.7 ± 0.2 2.1 ± 0.4	(1.2 ± 0.2) 3.6 ± 0.6	- 1.8 ± 0.1
interpretation	low symmetry incorporation species	disordered surface or near surface incorporation species	centro-symmetric incorporation species, coupled substitution (2 Ca ↔ Na/K+Eu)	locally ordered version of species C?

field splitting (twofold split F_1 band, and twofold split F_2 band) would be in line with a local D_3 symmetry and has been previously reported for Eu in a distorted perovskite structure [8]. The intensity ratio between F_1 and F_2 band suggests that species C, with the more intense magnetic dipole transition (F_1), is centro-symmetric, while species C', with a more intense electric dipole transition (F_2) is not [8]. One tentative explanation for species C' might be, that after the very slow formation of the Eu-calcite in this experiment local ordering occurs around the Eu-incorporation species. Such an ordering effect has previously been proposed by a theoretical study, suggesting that the relevant $EuNa(CO_3)_2$ endmember, which might be used in a thermodynamic model to describe the formation of species C, should have a dolomite like ordered structure [9]. Whether the proposed ordering may explain the observed crystal field splitting remains, however, to be clarified.

In summary, we identified four Eu species in calcite (neglecting for now the initial species identified in the kinetic experiment). The characteristics of these species are listed in Table 1. In our opinion it is possible to integrate our new results with previous findings and to develop a comprehensive mechanistic picture of Eu^{3+} incorporation into calcite. We suggest that Eu^{3+} interaction starts with the formation of a broad distribution of surface or near surface incorporation species (species D). Depending on time, interfacial kinetics (background electrolyte), Eu^{3+} concentration and solid/liquid ratio (i.e. Eu^{3+} surface coverage) species D evolves towards more well defined species: a sharper band of species D itself (cf. Fig. 2 and [4, 5]) and incorporation species B and C. Species D, but also species B seem to have a transitional character. Upon very slow calcite precipitation (aragonite to calcite transformation) we observe solely the formation of Species C, maybe accompanied by local ordering (Species C'). Note that after recrystallization experiments we hardly ever observe mono-exponential fluorescence decay behavior. We interpret the short-lived components of species B and C as overlap with species D.

Previously reported Species A seems to reflect special conditions in coprecipitation experiments at moderate supersaturation (SI(calcite) between 0.6 (vaterite–calcite recrystallization [4]) and ~1 (MFR [2, 10])) and low Eu^{3+} surface coverage. In MFR experiments at elevated Eu^{3+} concentration (results not shown) we observe the formation of Eu-species with broad excitation peaks, similar to Fig. 1 and similar to the nitrate experiments by Hofmann et al.. Thus, we tend to interpret the formation of well-defined species rather as being related to Eu^{3+} surface coverage and interfacial kinetics. We cannot reproduce the previously reported special effect of nitrate (cf Fig. 2). Concerning the effect of Na^+ vs. K^+, we confirm that species C is likely the result of coupled substitution (2 Ca ↔ Na/K+Eu). However, we consider the statement that Eu^{3+} incorporation in calcite is favored in the presence of Na^+ a misinterpretation (especially emphasized in [11]). There seems to be a slight shift from species C to species B in the presence of K^+. According to results reported by Marques et al. the overall Eu^{3+} uptake in calcite is, however, even slightly higher in the presence of K^+ compared to coprecipitation in the presence of Na^+.

Finally, our results indicate that over geologic periods of time species C will be the relevant incorporation species. In natural systems, usually sufficient Na^+ should be available to provide charge compensation. Especially if it should be possible to confirm the local ordering of species C and the consequent formation of species C', we are confident that it will be possible to develop a thermodynamic model for this long-term incorporation process based on DFT double-defect calculations [9] and few additional experiments. On the other hand, concerning the short-term effects observed in sorption and coprecipitation experiments, it will remain a major challenge to develop a comprehensive quantitative model recovering the various species in the various experiments (cf. also [12]).

X-ray spectroscopic investigations on structural iron in clay minerals

The encapsulation of nuclear waste in thick-walled cast-iron containers will result in an iron inventory exceeding by far that of e.g., uranium. The presence of high iron inventories may ultimately result in corrosion/alteration products containing structural iron. Specifically, structural iron in clay minerals can have a significant impact on the redox- and sorption capacity of clay minerals. Studies aiming at investigating the chemical status of structural iron in various mineral phases have been initiated in the group. Below are preliminary results obtained for structural iron present in two clay minerals: hectorite, a magnesian smectite frequently detected in glass corrosion experiments (e.g., [13]), and nontronite which is a smectite of high iron content.

Experimental details

Hectorite ($Na_{0.33}[Li_{0.33}Mg_{2.67}Si_4O_{10}(OH)_2]$) and nontronite ($Na_{0.5}[Fe_{3.0}Si_{3.5}Al_{0.5}O_{10}(OH)_2]$) were purchased from the Source Clay Repository, purified and the fraction < 0.1 µm separated by sedimentation and centrifugation techniques. XRD and FTIR data

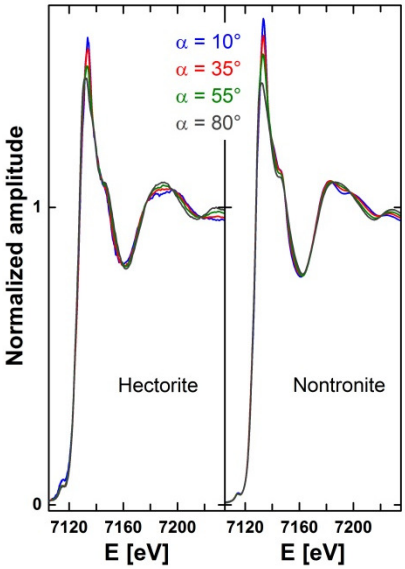

Fig. 5: *Experimental polarized XANES of hectorite (left) and nontronite (right).*

indicated the absence of any impurities. Both smectites were prepared as highly textured sample and the Fe local environment probed by polarized X-ray absorption spectroscopy at the INE beamline [14] at the synchrotron light source ANKA. Data were recorded considering various angles between the electric field of the X-ray beam and the clay layer plane (α = 10, 35, 55, 80°).

Results and interpretation

XANES can be used as fingerprint of the local chemical environment. The experimental XANES of hectorite differ from that of nontronite (Fig. 5) notably in the shape of the white line and in the first resonance centered at ~7200 eV, hinting at distinct short range environments. Both sets of polarized XANES exhibit clear angular dependences indicating that Fe is located in an anisotropic environment, and the decreasing amplitude with increasing angle α hints at an in-plane orientation of neighboring shells.

Both sets of polarized EXAFS spectra (Figure 6) exhibit significant angular dependences and contain several isosbestic points over the whole *k*-range. The spectra of hectorite differ from that of nontronite mostly in terms of position of the oscillation maxima, such as for example in the range $7 < k < 9$ Å^{-1}. Such frequencies as well as the change in oscillation maxima with increasing angle indicate the presence of backscattering shells located at different crystallographic positions within the structure.

The Fourier transforms (FT) also exhibit significant angular dependences (Figure 7). While the amplitude of the first contribution at $R + \Delta R$ ~1.7 Å decreases slightly, the increase in amplitude of the second FT peak of hectorite is remarkable. For nontronite, the amplitude of the first FT peak decreases and the amplitude of the second peak decreases while shifted to larger distances. This behavior indicates the presence of at least two atomic shells with distinct

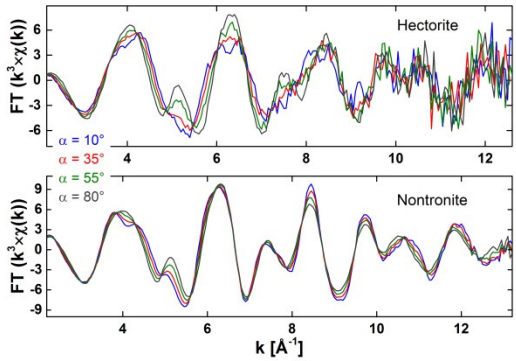

Fig. 6: *Experimental polarized EXAFS spectra of hectorite and nontronite.*

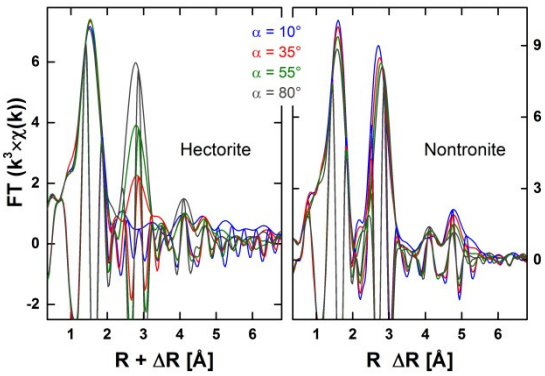

Fig. 7: *Experimental polarized Fourier transforms of spectra for hectorite (left) and nontronite (right).*

orientation, e.g., in-plane and out-of-plane orientation. For both smectites, the first FT peak is attributed to the first oxygen shell, preliminary fit results indicate the presence of 6 O atoms at ~2.00 Å. These fit results and the decrease in apparent coordination number with increasing angle are consistent with octahedral Fe^{3+} ions [15]. The next FT peak is due to contributions from neighboring octahedral and tetrahedral atoms. According to P-EXAFS, contributions in hectorite are significantly different from that in nontronite. Preliminary fit results indicate the presence of ~2 octahedral Mg and 4 tetrahedral Si atoms in hectorite. The low number of detected octahedral cations can originate either from a local dioctahedral environment or from an increased number of neighboring Li [16], an element too light to be detected by EXAFS spectroscopy. For nontronite, the detection of 3 octahedral Fe and 4 tetrahedral Si atoms agrees with earlier findings from Manceau et al. [15].

Further studies will focus on the characterization of structural iron as a function chemical composition of the octahedral and tetrahedral sheets.

References

[1] Lindqvist-Reis, P. et al., J. Phys. Chem. B, 110, (11), 5279-5285 (2006).
[2] Marques Fernandes, M. et al., J. Coll. Interface Sci., 321, 323-331 (2008).
[3] Kimura, T. et al., J. Alloys Comp., 213, 313-317 (1994).

[4] Schmidt, M. et al., J. Coll. Interface Sci., 351, (1), 50-56 (2010).
[5] Hellebrandt, S. et al., Sci. Rep., 6 (2016).
[6] Heberling, F. et al., Environ. Sci. Technol., 50, (21), 11735-11741 (2016).
[7] Ruiz-Agudo, E. et al., Geochim. Cosmochim. Acta, 75, (13), 3803-3814 (2011).
[8] Blasse, G. et al., J. Phys. Chem. Solids, 27, (10), 1587-1592 (1966).
[9] Vinograd, V. et al., Geochim. Cosmochim. Acta, 73, (13), A1386-A1386 (2009).
[10] Hofmann, S. et al., Geochim. Cosmochim. Acta, 125, 528-538 (2014).
[11] Schmidt, M. et al., Angew. Chem. Int. Edit., 47, (31), 5846-5850 (2008).
[12] Curti, E. et al., Geochim. Cosmochim. Acta, 69, (7), 1721-1737 (2005).
[13] Thien, B. et al., Appl. Clay Sci., 49, (3), 135-141 (2010).
[14] Rothe, J. et al., Rev. Sci. Instrum., 83, (4), 043105 (2012).
[15] Manceau, A. et al., Phys. Chem. Miner., 25, (5), 347-365 (1998).
[16] Finck, N. et al., Phys. Chem. Miner., 42, (10), 847-859 (2015).